Journal of Sound and Vibration 396 (2017) 246–254

Contents lists available at ScienceDirect

Journal of Sound and Vibration

journal homepage: www.elsevier.com/locate/jsvi

Inner detached frequency response curves: an experimental study

Gianluca Gatti [a,*], Michael J. Brennan [b]

[a] Department of Mechanical, Energy and Management Engineering, University of Calabria, 87036 Arcavacata di Rende, CS, Italy
[b] Departamento de Engenharia Mecânica, Universidade Estadual Paulista (UNESP), Ilha Solteira 15385-000, São Paulo, Brasil

ARTICLE INFO

Article history:
Received 4 October 2016
Received in revised form
21 December 2016
Accepted 6 February 2017
Handling Editor: Dr. M.P. Cartmell
Available online 23 February 2017

Keywords:
Detached resonance curve
Isolated resonance curve
Nonlinear vibration

ABSTRACT

Certain nonlinear vibrating systems have frequency response curves (FRCs), in which isolated detached curves exist inside the main continuous FRC. The behavior of these systems has hitherto been studied analytically and numerically, but to the authors' knowledge, there is no record of an inner detached FRC being detected experimentally. These curves may be hidden by numerical or experimental analysis, particularly when a system is subject to swept or stepped-sine excitation. Their existence may thus lead to unexpected dramatic changes in the amplitude of the system response. This paper presents an experimental study that involves the design, construction and testing of a specific system that has an isolated detached FRC inside the main continuous FRC. The experimental design of the test rig is supported by multibody dynamic simulations, and in the experimental tests the existence of a detached FRC was verified.

1. Introduction

One interesting feature of nonlinear oscillating systems is the multi-valuedness of their frequency response curves (FRCs) at some frequencies of excitation [1]. Specifically, in the case of harmonic excitation, and provided that the system response is predominantly harmonic at the excitation frequency, multiple solutions may appear in the steady-state amplitude response at a single frequency. Depending on the system configuration and on the values of the system parameters, closed detached resonance curves can appear either outside or inside the main continuous FRC.

Outer detached resonance curves have been predicted by several authors. For example, Starosvetsky and Gendelman [2] reported their theoretical prediction and numerical confirmation when analyzing the performance of a nonlinear vibration absorber attached to a linear host structure; they also predicted similar features when analyzing a three degrees-of-freedom (DOF) nonlinear oscillating system [3]. Alexander and Schilder [4] discovered a family of outer detached curves when analyzing the performance of a nonlinear tuned mass damper containing cubic stiffness nonlinearity. Outer detached curves have also been identified by Kerschen and co-workers [5,6] for the forced response of different nonlinear structures. More recently, isolated response regions outside the main continuous FRC have been shown to be also caused by internal resonances in simulations and experimental tests [7].

Inner detached resonance curves appear to have been first theoretically predicted and investigated by the authors of this paper and a co-worker [8] – they were validated numerically and named *bubbles* after their shape. By deriving approximate equations for the FRC of a harmonically excited system consisting of a coupled nonlinear and linear oscillator, the effect of

* Corresponding author.
E-mail addresses: gianluca.gatti@unical.it (G. Gatti), mjbrennan0@btinternet.com (M.J. Brennan).

http://dx.doi.org/10.1016/j.jsv.2017.02.008
0022-460X/

system parameters on their appearance was subsequently investigated [9,10]. The main restriction in their analysis, however, was a very low mass ratio between the nonlinear oscillator and the linear oscillator. This limitation meant that it was very difficult to design a test rig for experimental validation, as it became evident that isolated curves can only occur for a very narrow range of some of the system parameters [9].

Very recently, a comprehensive investigation on the detection of inner detached resonance curves has been reported by Gatti [11]. In this work, approximate analytical expressions for the FRC of a 2-DOF nonlinear oscillator were derived without any limitations on the mass ratio. Building on the previous analytical and numerical studies, this paper describes the design of a specific experimental rig, and subsequent tests to show conclusive evidence of an inner detached FRC in a 2-DOF system consisting of a coupled linear and nonlinear oscillator excited by a harmonic force. To design the test rig, a multibody model of the system was used to investigate the effect of un-modeled parameters in the analytical model, such as gravity, detailed geometry and rotational inertia, which could affect the dynamic behavior in a practical system.

The paper is organized as follows. Following this Introduction, an overview of the phenomenon of detached resonance curves is presented. Section 3 then describes the experimental design and Section 4 is devoted to a description of the experimental tests and results. The paper is concluded in Section 5. There is also an Appendix, which contains a resume of the pertinent results from reference [11].

2. Systems that have a detached FRC: an overview

Probably the simplest oscillating system where a detached FRC is theoretically predicted to occur, is a 2-DOF system, consisting of a linear spring-mass-damper system excited by a harmonic force, with an attached nonlinear oscillator having a linear plus cubic stiffness nonlinearity of the hardening type [8]. A schematic of such a system is shown in Fig. 1, whose equations of motion are given by

$$\begin{aligned} &m_s\ddot{x}_s + c_s\dot{x}_s + k_s x_s + c_1\dot{z} + k_1 z + k_3 z^3 = F\ \cos(\omega t) \\ &m\ddot{x}_s - m\ddot{z} - c_1\dot{z} - k_1 z - k_3 z^3 = 0 \end{aligned}, \tag{1a,b}$$

where m_s, k_s and c_s are the mass, stiffness and damping coefficient of the linear system, respectively; F and ω are the force amplitude and angular frequency of excitation, respectively; m and c_1 are the mass and damping coefficient of the attached nonlinear system, respectively; k_1 and k_3 are the linear and cubic stiffness coefficients, respectively; x_s and x are the displacements of the masses, and $z = x_s - x$ is the relative displacement; the overdots denote differentiation respect to time t.

In previous work [11], for small values of the damping ratios $\zeta_s = c_s/2m_s\omega_s$ and $\zeta = c_1/2m\omega_s$ (where $\omega_s = \sqrt{k_s/m_s}$), say less than about a few percent, it was found that two key non-dimensional parameters influence the condition that is necessary for the existence of an inner detached FRC. They are the mass ratio given by $\mu = m/m_s$, and the ratio between the natural frequency of the nonlinear attachment with $k_3 = 0$, to the natural frequency of the linear system alone, given by $\Omega_0 = \sqrt{k_1/(\mu k_s)}$. The necessary condition for the appearance (or not) of an inner detached FRC for an attachment with hardening stiffness nonlinearity is shown as a function of these two variables in Fig. 2, which is adapted from [11] – the meaning of the markers in this figure is given later. An inner detached FRC can potentially exist for the range of parameters corresponding to the white region of Fig. 2, while it will not exist for the combination of parameters corresponding to the shaded region. Note that an inner detached FRC may only exist when the natural frequency of the attachment (with $k_3 = 0$) is lower than the natural frequency of the linear system, and for relatively low values of the mass ratio. This occurs because

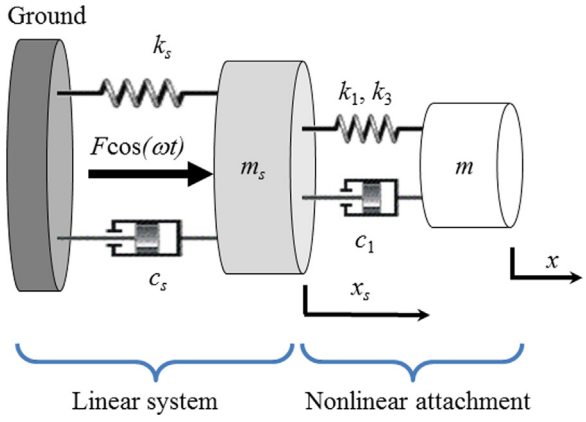

Fig. 1. Model of the 2-DOF nonlinear system under consideration.

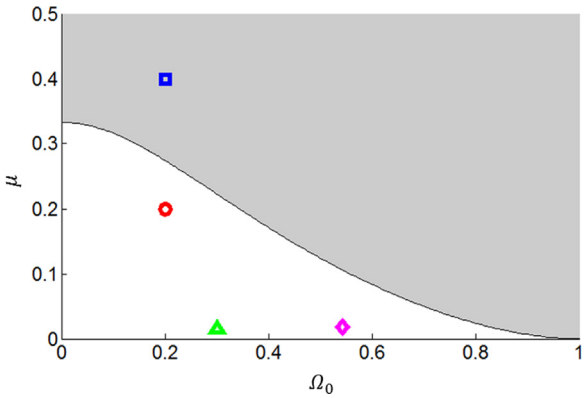

Fig. 2. Regions of the existence of a detached FRC in the $\Omega_0 - \mu$ plane [11]. For a combination of mass and frequency ratio inside the shaded region, no detached FRC is predicted. In the white region, detached FRCs can be predicted for hardening nonlinearity. The circle, square, triangle and diamond correspond, respectively, to a combination of $\mu = \Omega_0 = 0.2$, $\mu = 0.4$ and $\Omega_0 = 0.2$, $\mu = 0.015$ and $\Omega_0 = 0.3$, $\mu = 0.0188$ and $\Omega_0 = 0.543$.

when there is a light mass attachment, the hardening effect causes the FRC to bend the lower resonance peak to higher frequencies, so that it interacts with the other resonance peak to form the inner detached FRC. The reader is referred to reference [8] for more details concerning this phenomenon.

Provided that the parameters μ and Ω_0 are chosen correctly, then an inner detached FRC will form if the value of the nonlinear parameter $\gamma = k_3F^2/\mu k_s^3$ is within a specific range [11]. The upper limit of γ is given by [11]

$$\gamma_{\text{upper}} = -\frac{16\left(2\left(1+\sqrt{1+24\Omega_0^2}\right)+3\Omega_0^2\left(-9+\mu+\sqrt{1+24\Omega_0^2}+\mu\sqrt{1+24\Omega_0^2}\right)\right)^3}{2187\left(1+\sqrt{1+24\Omega_0^2}\right)^2\left(-5+\mu+\sqrt{1+24\Omega_0^2}+\mu\sqrt{1+24\Omega_0^2}\right)}, \tag{2}$$

but a relatively simple expression for the lower limit of γ is not known to exist. For parameter values of $\Omega_0 = \mu = 0.2$, the range of γ for an inner detached FRC to occur is found to be approximately $0.020 < \gamma < 0.025$.

To help in visualizing the effect of the nonlinear parameter γ on the FRC, two animations are attached. Video 1 shows the effect of increasing the non-dimensional nonlinear parameter γ, for $\Omega_0 = \mu = 0.2$ (the circle in Fig. 2), and Video 2 shows the same effect for $\Omega_0 = 0.2$, $\mu = 0.4$(the square in Fig. 2). It can be seen that an inner detached FRC is only formed in Video 1, for values of γ in the approximate range of $0.020 < \gamma < 0.025$.

Supplementary material related to this article can be found online at http://dx.doi.org/10.1016/j.jsv.2017.02.008.

Examples of the FRCs for the system are plotted in Fig. 3(a) and (b) for the specific value of $\gamma = 0.022$, and for $\Omega_0 = \mu = 0.2$ and $\Omega_0 = 0.2$, $\mu = 0.4$, respectively. They are calculated using the analytical expressions derived in [11] which are given in the Appendix for ease of reference. In the figures, the solid lines denote stable harmonic solutions, the dashed lines denote

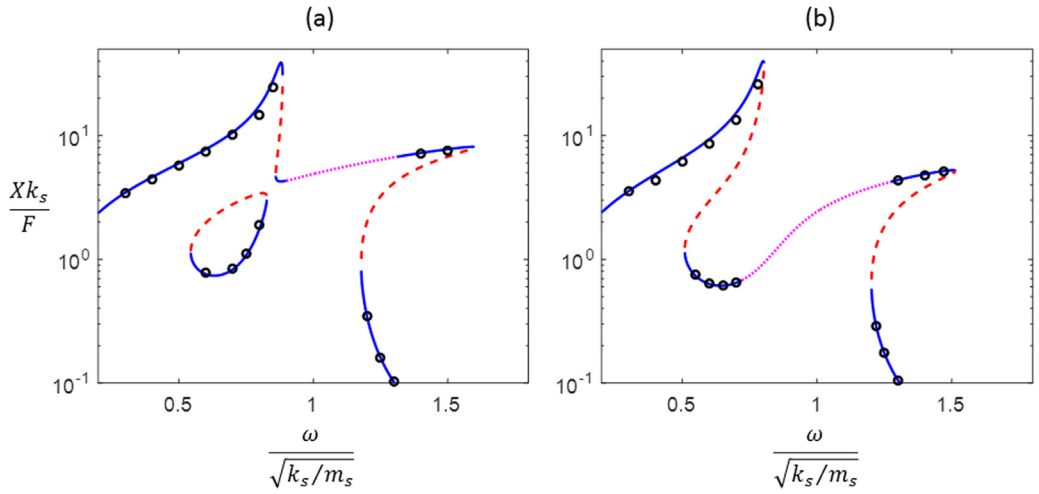

Fig. 3. FRC of the non-dimensional displacement amplitude of the suspended mass for (a) $\mu = \Omega_0 = 0.2$(circle in Fig. 2), and (b) $\mu = 0.4$,$\Omega_0 = 0.2$(square in Fig. 2), for $\zeta_s = 0.02$, $\zeta = 0.03$ and $\gamma = 0.022$. Stable analytical solutions (solid lines), unstable analytical solutions (dashed lines), quasi-periodic solution (dotted lines), numerical solutions (circles).

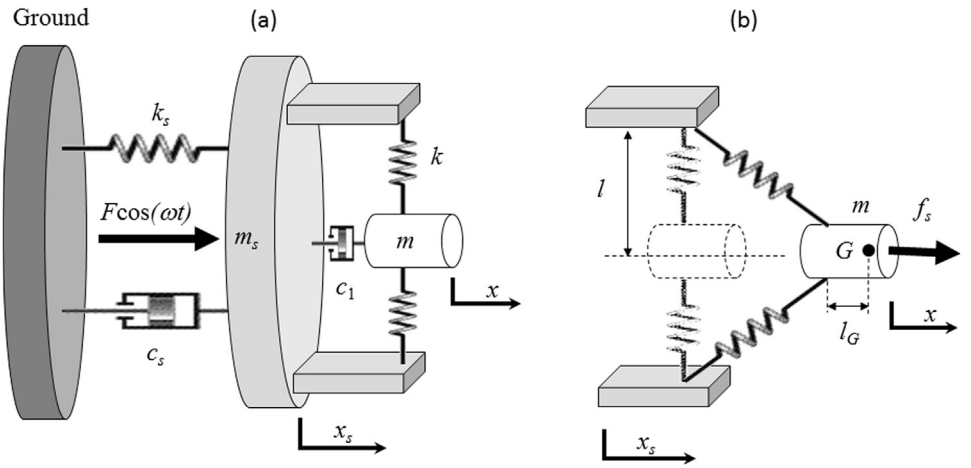

Fig. 4. (a) Practical configuration of the 2-DOF nonlinear system and (b) detail of the nonlinear attachment.

unstable solutions and the dotted lines denote quasi-periodic solutions. Also plotted in the figures are circles corresponding to the first harmonic of the solution to the equations of motion obtained numerically. The "birth" of the inner detached FRC can be seen in Fig. 3(a), whereas it does not form in Fig. 3(b) for the same values of γ and Ω_0, but with a different value of μ(as predicted from Fig. 2).

3. Design of the test structure

One way of achieving a mechanical system that behaves in accordance with the mathematical description given by Eq. (1a,b), is to arrange linear springs of stiffness k as shown in Fig. 4(a). A close-up of the motion of the attached mass m, is shown in Fig. 4(b). It can be seen that when the mass is displaced in the horizontal direction, the springs incline, causing a hardening stiffness characteristic [8]. For n pairs of springs, the relationship between the static force f_s in Fig. 4(b) and the resulting relative displacement z, is given by

$$f_s = nkz\left(1 - \frac{l_0}{\sqrt{z^2 + l^2}}\right) \tag{3}$$

where l is the length of each spring in the nonlinear attachment when assembled, and $l_0 < l$ is the length of the un-stretched spring. Applying the Maclaurin expansion to the third order for a small relative displacement, Eq. (3) can be written as

$$f_s \approx k_1 z + k_3 z^3 \tag{4a}$$

where

$$k_1 = 2nk(1 - l_0/l), \tag{4b}$$

$$k_3 = nkl_0/l^3. \tag{4c}$$

Note that Eq. (4a) is the static restoring force in Eq. (1a,b).

An experimental rig with $n = 2$ was studied in [12] to explore the performance of a nonlinear vibration neutralizer. In that case, the assumption was that the frequency of excitation (at which the system response was to be attenuated) was much higher than the natural frequency of the host system, so that no interaction of the two resonance peaks was expected. This condition was achieved by tightening the springs k in tension when assembled. Fig. 5(a) depicts a photograph of the experimental rig studied in [12]. This configuration is used here to illustrate some of the practical issues involved in the design of a system that exhibits an inner detached FRC. In Fig. 5(a), the electrodynamic shaker acts as a linear oscillator and provides the harmonic force excitation. The neutralizer is the nonlinear attachment. The system parameters considered here are given in Table 1, and the corresponding values of the mass and frequency ratio are $\mu = 0.015$ and $\Omega_0 = 0.3$, respectively. They correspond to the triangle in Fig. 2. For the parameters listed in Table 1, the FRC of the suspended mass is plotted in Fig. 6(a) using the analytical model together with numerical validation. Note that there is good agreement between the analytical model and the numerical simulation.

To determine the effects of some important practical details of a 2-DOF system that cannot be captured with a relatively simple analytical model, a multibody model is developed of the system shown in Fig. 5(a) using the software SimMechanics™. It is shown in Fig. 5(b). This model is used to investigate the effects of un-modelled parameters in the

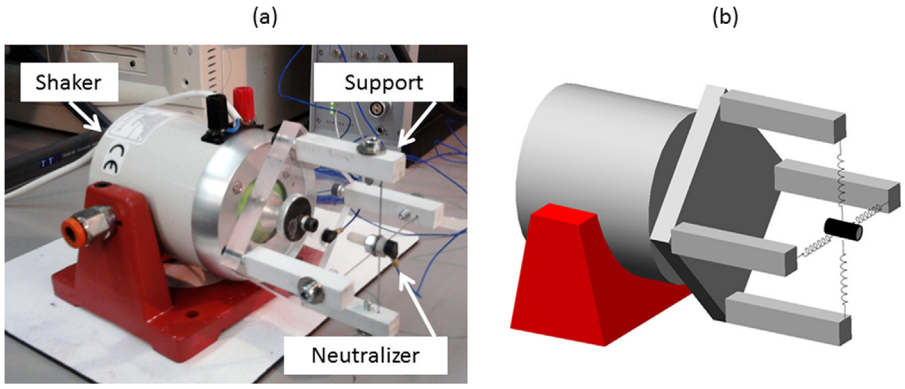

Fig. 5. Photograph and schematic of a vibration neutralizer attached to an electrodynamic shaker for testing [12]: (a) photograph and (b) multibody model. In this paper the complete system is considered; the shaker is the linear system, and the neutralizer is the nonlinear attachment.

Table 1
Dynamic parameters of the physical system in Fig. 5(a).

F [N]	m_s [kg]	k_s [N/m]	c_s [N s/m]	m [kg]	k_1 [N/m]	k_3 [N/m^3]	c_1 [N s/m]
1.11	0.20	1.00×10^4	7.55	0.003	14.12	6.92×10^7	0.026

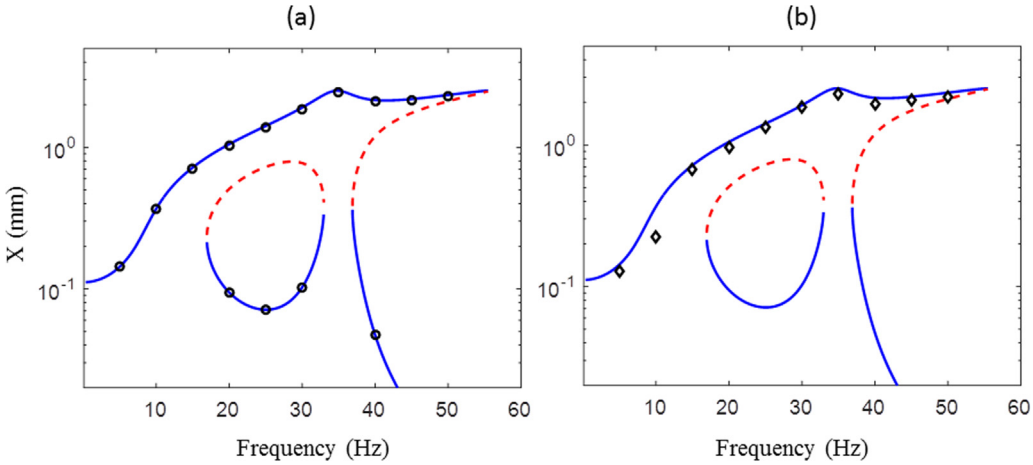

Fig. 6. FRC of the displacement amplitude of the suspended mass for the parameters reported in Table 1. Stable analytical solutions (solid lines), unstable analytical solutions (dashed lines). The circles in (a) correspond to the numerical solutions obtained by integrating the equation of motion Eq. (1a,b), and the diamonds in (b) correspond to the numerical solutions obtained by the multibody simulation with geometric parameters reported in Table 2.

analytical model, such as gravity and the rotational inertia of the suspended mass. The suspended mass is modelled as a solid cylinder with length l_m and diameter d_m. The lateral springs are pinned at the outer surface of the cylindrical body, and its center of mass G is defined relative to the intersection point of the attached lateral springs by an offset l_G, as shown in Fig. 4(b). The geometrical parameters are given in Table 2. Simulations are performed starting from rest, until the response reaches steady-state. The numerical results from the multibody simulations are shown in Fig. 6(b) as diamonds, together with the FRC calculated from the analytical model. As can be seen, no solution is obtained in the lower stable branch of the detached FRC, and at higher frequencies (above approximately 36 Hz), where no harmonic solution is found on the lower stable branch. This behavior is thought to be related to the unfavorable combination of gravity, suspended mass unbalance

Table 2
Geometric parameters used in the simulations for the multibody model in Fig. 5(b).

l [m]	l_0 [m]	l_m [m]	d_m [m]	l_G [m]
0.034	0.033997	0.015	0.006	$l_m/4$

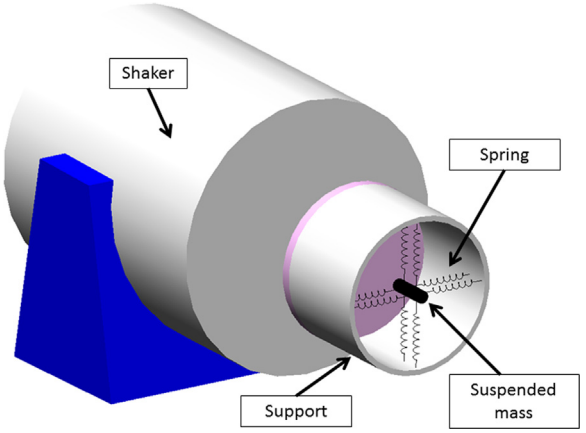

Fig. 7. Multibody model of the mechanical prototype used for experimental tests.

and relatively small linear stiffness coefficient k_1, which induces an undesirable wobbling motion of the suspended mass, which was discussed in some detail by the authors in [13].

One way to reduce the undesirable wobbling behavior of the mass is to design a suspended mass with a smaller length to diameter ratio, and perhaps use a disc-type or ring-type mass, as described in [8]. However, such a solution would have a profound effect on the mechanical design of the whole system, because the nonlinear coefficient k_3 is dependent on the cube of the spring length. Thus, to achieve the same nonlinear effect, the support structure would need to be enlarged (with a likely increase in weight), which would affect both the mass ratio and the shaker specifications.

Another way to reduce the undesirable wobbling is to use an additional set of springs as shown in Fig. 7. Here, two sets of four springs are used in parallel (i.e. $n = 4$) to limit the wobbling motion due to gravity and unbalance. The multibody simulations performed on such configuration confirmed the effectiveness of such a design strategy, and the results obtained overlaid those shown in Fig. 6(a) as circles.

4. Experimental work

In an attempt to detect the inner detached FRC experimentally, a test-rig was designed based on the multibody model depicted in Fig. 7, and is shown in Fig. 8(a). It consists of an electrodynamic shaker (Tira S514), which acts as the linear system shown in Fig. 1, to which the nonlinear oscillator is attached. The nonlinear attachment is shown in more detail in Fig. 8(b). It consists of a round plastic container with a threaded lid, acting as a support for the suspended mass. For assembly purposes, the container lid is first bolted to the shaker head, and the container is then screwed on to its lid. The suspended mass is made from a cylindrical transparent plastic tube (corresponding to the black small cylinder in Fig. 7) and is suspended by a parallel combination of fishing lines, which act as the springs depicted in the model of Fig. 7.

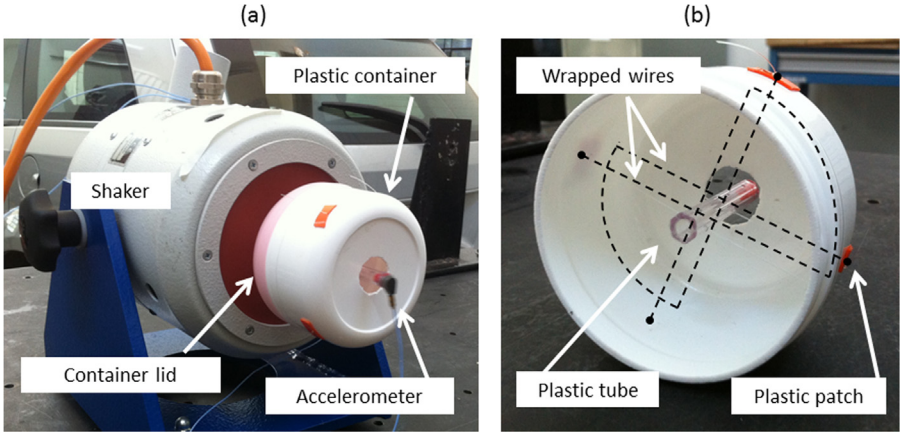

Fig. 8. Experimental prototype used for the tests: (a) photograph of the rig, and (b) detail of the nonlinear attachment.

Table 3
Dynamic parameters of the mechanical prototype in Fig. 8.

F [N]	m_s [kg]	k_s [N/m]	c_s [N s/m]	m [kg]	k_1 [N/m]	k_3 [N/m^3]	c_1 [N s/m]
1.8	0.32	1.37×10^4	1.96	0.006	75.69	2.26×10^7	0.01

An accelerometer (PCB 352A25) was attached to one extreme of the suspended mass as shown in Fig. 8(a). The shaker was connected to a power amplifier (Tira BAA500), which was driven by an LMS SCADAS signal generator and acquisition system. The parameters of the linear system were obtained through a single DOF linear fitting to the measured frequency response of the shaker alone. The suspended mass with accelerometer was weighted independently, the nominal diameter of the fishing line was $d_w = 0.3 \times 10^{-3}$ m and its Young's modulus was considered to be equal to the conventional value for nylon, i.e. $E = 3 \times 10^9$ N/m^2. The diameter of the plastic container was $D = 0.075$ m, and the diameter of the suspended plastic tube was $d_m = 8 \times 10^{-3}$ m. To assure uniform tension for the springs modelled in Fig. 7, only one piece of fishing wire was used for each set of co-planar springs. The wire was wrapped around the plastic container as detailed in Fig. 8(b). When assembled, the length of each spring was $l = (D - d_m)/2 = 0.0335$ m, and the un-stretched length l_0 was estimated by assuming uniform deformation ε along the entire wire, i.e.,

$$\varepsilon = \frac{l - l_0}{l_0} \approx \frac{\Delta}{l_w}, \tag{5}$$

where $l_w = (2 + \pi/4)D \approx 0.2$ m is the total length of each wrapped wire, and Δ is the change in length when assembled, which was measured as $\Delta \approx 0.3 \times 10^{-3}$ m. Plastic patches of known thickness were used to provide a measurable value for Δ, and these red patches are shown on the surface of the round plastic container in Fig. 8(a) and (b). From Eq. (5), the un-stretched spring length was then estimated to be $l_0 = 0.03345$ m. The stiffness of each spring was finally calculated to be $k = E\pi d_w^2/4l_0$ and the linear and nonlinear stiffness coefficients were calculated using Eqs. (4b) and (4c), respectively. The damping in the attachment was not estimated, but set to a value of $c_1 = 0.01$ N s/m, which corresponds to the damping ratio estimated in [12] for a similar system. All the parameters of the experimental rig illustrated in Fig. 8 are given in Table 3. Using these measured or estimated parameters gives a mass and frequency ratio of $\mu = 0.0188$ and $\Omega_0 = 0.543$, respectively, and correspond to the diamond shown in Fig. 2. The FRC of the acceleration of the suspended mass predicted using the analytical model is shown in Fig. 9.

For the test set-up, a stepped-sine input was used to drive the shaker in current mode, with a frequency step of 0.1 Hz. Three tests were performed, with all of them starting from rest. In the first test, the initial frequency of the stepped-sine was 15 Hz, and the final frequency was 40 Hz. The corresponding results are shown in Fig. 9 as yellow squares. It can be seen that the experimental data follows the upper branch of the FRC, until a jump-down occurs at about 36 Hz, which is due to an instability in the harmonic solution. In the second test, the initial frequency was 24 Hz and the final frequency was 32 Hz. The results of this test are shown in Fig. 9 as right-pointing cyan triangles. Note that the experimental FRC started on the

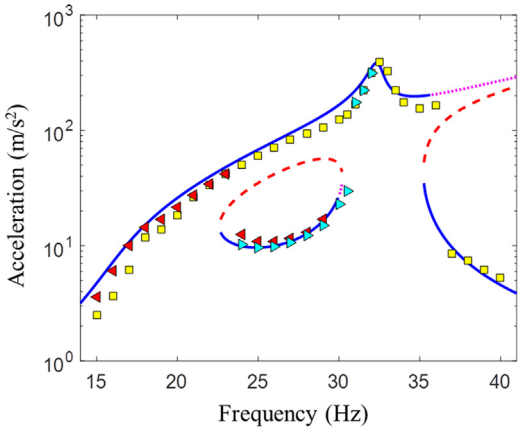

Fig. 9. FRC of the acceleration amplitude of the suspended mass. Stable analytical solutions (solid lines), unstable analytical solutions (dashed lines), quasi-periodic solution (dotted lines), calculated for the parameters reported in Table 3. Experimental results for the experimental rig in Fig. 8 due to a stepped-sine excitation (a) from 15 to 40 Hz (squares), (b) from 24 to 32 Hz (right-pointing triangles), (c) from 29 to 15 Hz (left-pointing triangles).

lower branch belonging to the inner detached FRC, staying on that branch until it jumped-up to the higher branch of the main continuous curve at a frequency of about 30 Hz. The third test involved a decrease in frequency from 29 Hz to 15 Hz, and the corresponding results are shown in Fig. 9 as left-pointing red triangles. In this case, again, the experimental FRC started on the lower branch belonging to the inner detached FRC, staying on that branch until it jumped-up to the higher branch at a frequency of about 24 Hz. Examining Fig. 9, it can be clearly seen that the experimental results compare well with the theoretical predictions.

It is speculated that the lower branch of the detached curve was found in each case because it is an "inner" detached curve, and as such, its branch is at a lower amplitude than the main continuous response curve. This may not be the case for an "outer" detached curve, which appears outside the main continuous response curve, and as such, usually has a higher amplitude, which can be more difficult to reach.

5. Conclusions

This paper has described the conditions under which an inner detached FRC will occur in practice. Experimental evidence has been presented to show the appearance of an inner detached FRC curve in the main frequency response of a two-degrees-of-freedom nonlinear oscillator. The experimental set-up consisted of (a) an electrodynamic shaker, acting as a linear mass-spring-damper system excited by a harmonic force with constant amplitude, and (b) a nonlinear oscillator attached to its moving head via a support structure, through a combination of linear springs connected in such a way as to achieve a hardening stiffness nonlinearity. The range of parameters and specific geometry required to achieve a system with an inner detached FRC has been discussed, and these conditions have been applied in the design of the experimental test-rig using multibody dynamics software. In particular, it was observed that the unfavorable combination of gravity, weight unbalance and quasi-zero stiffness characteristic of the nonlinear attachment plays an important role in the system dynamics, and could prevent the occurrence of inner detached FRCs.

Stepped-sine excitation was used in the experimental tests, and the results showed very good agreement with the analytical prediction, in particular with the vibration levels of the main continuous FRC and the inner detached FRC, as well as the jump frequencies between these curves.

Isolated response curves have received increasing attention in recent years as pointed out in a recent review paper by Noël and Kerschen [14]. The practical demonstration of such features in this paper, could pave the way to their potential application by the engineering community, who are trying to take advantage of nonlinearity rather than avoiding it.

Acknowledgment

The authors acknowledge the support of FAPESP Research Award 15/19614-4.

Appendix A

This Appendix gives the non-dimensional form of the equations of motion shown in Eq. (1a,b) and their solution, as reported in [11]. The equations are used to plot the FRCs. Given the non-dimensional parameters ζ_s, ζ, μ, Ω_0 and γ, as defined in Section 2, the non-dimensional equations of motion of the system shown in Fig. 1 may be written as

$$y_s''(1+\mu) + 2\zeta_s y_s' + y_s = \cos(\Omega\tau) + \mu w'' \tag{A.1}$$

$$w'' + 2\zeta w' + \Omega_0^2 w + \gamma w^3 = y_s'', \tag{A.2}$$

where $y_s = x_s k_s/F$, $w = z k_s/F$, $\Omega = \omega/\omega_s$ in which $\omega_s = \sqrt{k_s/m_s}$, and $(\cdot)' = d(\cdot)/d\tau$, in which $\tau = \omega_s t$ is non-dimensional time. Note also that $y = x k_s/F$ is the non-dimensional displacement of mass m. As described in [11], when the excitation is harmonic, the amplitude-frequency relations corresponding to Eqs. (A.1) and (A.2) can be derived, and are given by

$$a\gamma^2 W^6 + b\gamma W^4 + cW^2 + d = 0 \tag{A.3}$$

$$Y_s^2 = \frac{1 - W^4 g - W^2 h}{e} \tag{A.4}$$

$$Y^2 = \left(Y_s \cos(\varphi_s) - W \cos(\varphi)\right)^2 + \left(Y_s \sin(\varphi_s) - W \sin(\varphi)\right)^2, \tag{A.5}$$

where

$$a = \frac{9}{16}$$
$$b = \frac{3}{2}\left(\Omega_0^2 - \Omega^2\right) + \Omega^4\frac{g}{e}$$
$$c = \left(\Omega_0^2 - \Omega^2\right)^2 + 4\zeta^2\Omega^2 + \Omega^4\frac{h}{e}$$
$$d = -\frac{\Omega^4}{e}$$
$$e = \left(1 - \Omega^2(1+\mu)\right)^2 + 4\zeta_s^2\Omega^2$$
$$g = -\frac{3}{2}\mu\left(1 - \Omega^2(1+\mu)\right)$$
$$h = \Omega^4\mu^2 - 2\mu\left(1 - \Omega^2(1+\mu)\right)\left(\Omega_0^2 - \Omega^2\right) + 8\zeta\zeta_s\mu\Omega^2,$$

and Y_s, Y and W are the amplitudes of the displacements of the two masses and the relative displacement between them, respectively; φ_s is the phase of the displacement of mass m_s, which can be determined from

$$\cos(\varphi_s) = Y_s\left(1 - \Omega^2(1+\mu)\right) + \Omega^2\mu W\ \cos(\Delta\varphi) \tag{A.6a}$$
$$\sin(\varphi_s) = -2\zeta_s\Omega Y_s + \Omega^2\mu W\ \sin(\Delta\varphi); \tag{A.6b}$$

φ is the phase of the displacement of mass m, which can be determined from

$$\cos(\varphi) = \cos(\Delta\varphi)\cos(\varphi_s) + \sin(\Delta\varphi)\sin(\varphi_s) \tag{A.7a}$$
$$\sin(\varphi) = \cos(\Delta\varphi)\sin(\varphi_s) - \sin(\Delta\varphi)\cos(\varphi_s); \tag{A.7b}$$

and the difference in phase $\Delta\varphi = \varphi_s - \varphi$ is given by

$$\cos(\Delta\varphi) = \frac{-W}{\Omega^2 Y_s}\left(\Omega_0^2 - \Omega^2 + \frac{3}{4}\gamma W^2\right) \tag{A.8a}$$
$$\sin(\Delta\varphi) = \frac{-2\zeta W}{\Omega\ Y_s}. \tag{A.8b}$$

References

[1] A.H. Nayfeh, B. Balachandran, *Applied Nonlinear Dynamics*, Wiley, New York, 1995.
[2] Y. Starosvetsky, O.V. Gendelman, Vibration absorption in systems with a nonlinear energy sink: nonlinear damping, *J. Sound Vib.* 324 (2009) 916–939.
[3] Y. Starosvetsky, O.V. Gendelman, Dynamics of a strongly nonlinear vibration absorber coupled to a harmonically excited two-degree-of-freedom system, *J. Sound Vib.* 312 (2008) 234–256.
[4] N.A. Alexander, F. Schilder, Exploring the performance of a nonlinear tuned mass damper, *J. Sound Vib.* 319 (2009) 445–462.
[5] T. Detroux, L. Renson, L. Masset, G. Kerschen, The harmonic balance method for bifurcation analysis of large-scale nonlinear mechanical systems, *Comput. Methods Appl. Mech. Eng.* 296 (2015) 18–38.
[6] R.J. Kuether, L. Renson, T. Detroux, C. Grappasonni, G. Kerschen, M.S. Allen, Nonlinear normal modes, modal interactions and isolated resonance curves, *J. Sound Vib.* 351 (2015) 299–310.
[7] A.D. Shaw, T.L. Hill, S.A. Neild, M.I. Friswell, Periodic responses of a structure with 3:1 internal resonance, *Mech. Syst. Signal Process.* 81 (2016) 19–34.
[8] G. Gatti, M.J. Brennan, I. Kovacic, On the interaction of the responses at the resonance frequencies of a nonlinear two degree-of-freedom system, *Physica D: Nonlinear Phenom.* 239 (2010) 591–599.
[9] G. Gatti, I. Kovacic, M.J. Brennan, On the response of a harmonically excited two degree-of-freedom system consisting of a linear and a nonlinear quasi-zero stiffness oscillator, *J. Sound Vib.* 329 (2010) 1823–1835.
[10] G. Gatti, M.J. Brennan, On the effects of system parameters on the response of a harmonically excited system consisting of weakly coupled nonlinear and linear oscillators, *J. Sound Vib.* 330 (2011) 4538–4550.
[11] G. Gatti, Uncovering inner detached resonance curves in coupled oscillators with nonlinearity, *J. Sound Vib.* 372 (2016) 239–254.
[12] M.J. Brennan, G. Gatti, The characteristics of a nonlinear vibration neutralizer, *J. Sound Vib.* 331 (2012) 3158–3171.
[13] G. Gatti, S. Marchesiello, M.J. Brennan, A virtual experiment for the detection of specific features in the frequency response of a coupled nonlinear and linear oscillator, in: Proceedings of the IX International Conference on Structural Dynamics, Porto, Portugal, June 30–July 2, 2014.
[14] J.P. Noël, G. Kerschen, Nonlinear system identification in structural dynamics: 10 more years of progress, *Mech. Syst. Signal Process.* 83 (2017) 2–35.